Materials Science and Engineering B 177 (2012) 1460–1464

Contents lists available at SciVerse ScienceDirect

Materials Science and Engineering B

journal homepage: www.elsevier.com/locate/mseb

Short communication

CdSe/CdTe interface band gaps and band offsets calculated using spin–orbit and self-energy corrections

M. Ribeiro Jr.[a,*], L.G. Ferreira[b], L.R.C. Fonseca[c], R. Ramprasad[d]

[a] Centro de Pesquisas Avançadas Wernher von Braun, Av. Alice de Castro P.N. Mattosinho 301, CEP 13098-392 Campinas, SP, Brazil
[b] Departamento de Física dos Materiais e Mecânica, Instituto de Física, Universidade de São Paulo, 05315-970 São Paulo, SP, Brazil
[c] Center for Semiconductor Components, State University of Campinas, R. Pandia Calógeras 90, 13083-870 Campinas, SP, Brazil
[d] Department of Chemical, Materials and Biomolecular Engineering, Institute of Materials Science, University of Connecticut, 97 North Eagleville Road, Storrs, CT 06269, USA

ARTICLE INFO

Article history:
Received 10 October 2011
Received in revised form
14 December 2011
Accepted 23 December 2011
Available online 9 January 2012

Keywords:
Band gap
Band offset
Density functional theory
Excited states
Photovoltaic materials

ABSTRACT

We performed *ab initio* calculations of the electronic structures of bulk CdSe and CdTe, and their interface band alignments on the CdSe in-plane lattice parameters. For this, we employed the LDA-1/2 self-energy correction scheme [L.G. Ferreira, M. Marques, L.K. Teles, Phys. Rev. B 78 (2008) 125116] to obtain corrected band gaps and band offsets. Our calculations include the spin–orbit effects for the bulk cases, which have shown to be of importance for the equilibrium systems and are possibly degraded in these strained semiconductors. Therefore, the SO showed reduced importance for the band alignment of this particular system. Moreover, the electronic structure calculated along the transition region across the CdSe/CdTe interface shows an interesting non-monotonic variation of the band gap in the range 0.8–1.8 eV, which may enhance the absorption of light for corresponding frequencies at the interface between these two materials in photovoltaic applications.

1. Introduction

Energy is a great challenge for the next decades, provided the fossil fuel-derived sources emissions of large amounts of CO_2 are increasing, with associated anthropogenic greenhouse effects. As an alternative to go beyond silicon efficiency, photovoltaic materials in nanostructured phases have been studied, like quantum films, wires and dots to improve efficiency of solar energy harvesting and conversion [1–3]. With the increasing advances in solid state fabrication techniques for nanostructures [4,5], the simulation techniques play an important role as systems approach the atomic scale. Density functional theory together with local density approximation [6,7] has been the main theoretical tool in condensed matter simulation, and has a widespread application in nanostructures [8]. For the case of photovoltaic materials, there is a need to understand and predict the valence and conduction staggered band alignments. However, a major challenge comes from the fundamental difficulties to predict the band gaps theoretically, in particular for large systems due to computational costs involved. It is well known that density functional theory (DFT) fails to predict excited state properties of materials [9], what forces most researchers to use (i) adjustable parameters or semi-empirical methods and/or (ii) simplified models to accurately describe experimental findings. This becomes a drawback to the study of potentially efficient photovoltaic materials [10], which are still not characterised or optimised. *State-of-the-art* methodologies like *GW* to improve the description of excited states have been used for the photovoltaic CdSe/CdTe system [11] as well as to bulk and surfaced CdTe system [12]. In this work, we intend to show how a newly developed technique, called LDA-1/2 [13,14], deals with this particular problem of the CdSe/CdTe photovoltaic interface and predicts that proper band alignment feature. The LDA-1/2 method has been very successful in this type of calculation for other interfaces [15,16]. We modelled II–VI CdSe and CdTe semiconductors in wurtzite (wz, $P6_3mc$) structure as a CdSe/CdTe interface to calculate the band gaps and band offsets. This setup was motivated by applications of these systems in core/shell (0 0 0 1) CdSe/CdTe nanowires under strain as described in Ref. [17], though there are known differences in the dependence of the band gap on strain between bulk and nanostructures[10]. Although recent work shows that the improvement of this type of material involves theoretical understanding of defects and their formation mechanisms [18], our interface is made without point defects, being all the possible effects in band structure introduced by strain. For thin enough films, lattice-mismatched heterostructures can be grown without misfit defects as first studied by Matthews and Blakeslee [19]. Because the strain for our interfaces is about 6.4 % (which differs somewhat from the hexagonal interface found in very thin nanowires [10]), the defect-free approximation in only realistic for films a few

* Corresponding author. Tel.: +55 1132622207; fax: +55 1132622207.

0921-5107/$ – see front matter © 2012 Elsevier B.V. All rights reserved.
doi:10.1016/j.mseb.2011.12.044

Table 1
Bulk and strained LDA lattice vectors for wz–CdSe and wz–CdTe. *str* LDA values refer to CdTe strained to the CdSe *c* and *a* lattice vectors. Experimental values taken from Ref. [25].

	Lattice vectors (Å)				
	CdTe			CdSe	
	LDA	*str* LDA	Exp.	LDA	Exp.
a	4.52	4.64	4.58	4.24	4.30
c	7.42	6.95	7.50	6.95	7.02

atomic layers thick, [20] which is the case in this study. To enrich the discussions, we also analyse the impact of spin–orbit effects with common LDA and LDA-1/2 on bulk unstrained CdSe and CdTe, as well as their possible implications on the band offsets.

2. Methods

Our total-energy and electronic structure calculations were based on the DFT within the local density approximation (LDA) of Perdew and Zunger [21]. For the description of the interactions among electrons and nuclei we used the frozen-core projector augmented-wave (PAW)[22] *ab initio* pseudopotentials (PP) as implemented in the "Vienna *Ab-initio* Simulation Package" (VASP-PAW code) [23]. The cutoff for the plane wave expansion was 274 eV. The *k*-space integrals were approximated by sums over a special mesh of the Monkhorst–Pack (MP) type [24] in the irreducible part of the Brillouin zone (BZ). For bulk and slab calculations we used $9 \times 9 \times 9$ and $9 \times 9 \times 1$ MP *k*-meshes respectively, both including the Gamma point, and a denser $12 \times 12 \times 1$ mesh for the density of states calculations. To account for the band splittings at the valence band maximum (VBM) of each bulk material we included the spin–orbit (SO) coupling explicitly in the calculations, thus making the energy dependent on the direction of the magnetic moment. As shown below, the SO splitting is of considerable importance to the reproduction of experimental band gaps. The impact of SO splittings was evaluated as shifts in band offsets energies in our slab calculations *a posteriori* as rigid shifts of the valence band edges (VBE) with values given by the calculated bulk strained band splittings.

Our calculated bulk lattice vectors (LV) shown in Table 1 are within 1.5% and 1.4% (1.5% and 1.6%) of the experimental values for the *a* (*c*) LV of wz–CdTe and wz–CdSe, respectively, which is typical of well-converged LDA structural parameters. The wurtzite heterostructure supercell was built with normal vectors and the *c* LV parallel to the plane of the junction. Ahead we give some more details about the model structure used as supercell. The $a_{\parallel}$ (lattice vector parallel to the interface) and *c* LVs of the CdTe slab were fit to the CdTe slab values, while the normal LV $a_{\perp}$ was relaxed, partially relieving the strain energy. The heterostructure with the interface LVs set to the calculated bulk values of CdSe had the LV values of $\{a_{\parallel}$=4.24Å; $a_{\perp}$=123.04Å; *c*=6.95Å$\}$. The LV $a_{\perp}$ of the strained slab is relaxed to minimise the strain energy.

To improve on the LDA underestimation of band gaps, we employed the LDA-1/2 method [13]. Our intention is to correct the band gaps to improve the band alignment of the interface. The LDA-1/2 method has shown excellent results for band gaps [13,14,26] and band offsets [15,16]. The LDA-1/2 method follows from Slater's half-ionisation technique [27,28] which yields excellent results for the ionisation potentials of atoms. Is possible to demonstrate the connection with the self-energy (electrostatic) in the expression of the second derivative of Janak's theorem, and then extend the idea to crystals, in which one adds to the crystalline potential an atomic "self-energy potential" V_S, defined as the difference between the Kohn-Sham atomic potential and that of the half-ion, $V_S(r) = V(0, r) - V(-1/2, r)$. Here the first index in the potential *V* refers to the occupation number, *r* being the radius in atomic units. In general, only the anionic self-energy potential is important because the valence band, composed mostly of anion states, is more localised than the conduction band and therefore has larger self-energy. We found that only modifying the Se and Te *p*-orbitals proved necessary. Because the self-energy is local, the long-range Coulomb potential tail needs to be bounded by a cutoff radius (CUT) to avoid overlapping with the self-energy potentials of the other anions in the lattice. This procedure is done by multiplying the self-energy potential by a cutoff function $\Theta(r)$, defined as follows

$$\Theta(r) = \begin{cases} \left[\left(1 - \dfrac{r}{\mathrm{CUT}}\right)^m\right]^3 & , \text{if } r \le \mathrm{CUT} \\ 0 & , \text{if } r > \mathrm{CUT} \end{cases} \quad (1)$$

so that we can make a variational procedure to find the optimal CUT value doing a calculation of E_g(CUT). This procedure makes the method free of adjustable parameters [13]. In Eq. (1) the exponent *m* shall be made as large as possible so that the cutoff is sharp but without introducing numerical problems. To obtain the final band structure for this system, one more self-consistent calculation with atomic positions fixed is necessary. Therefore, no considerable computational effort is done with LDA-1/2 if compared to LDA. Fig. 1 shows the optimisation of the CUT parameter for Se and Te. The optimal CUT values are found at the maximum of the bulk band gaps, with values 3.7 and 4.0 atomic units (a.u.) for the Se and Te *p*-orbitals, respectively. All LDA-1/2 calculations were performed with LDA-relaxed LVs (see Table 1).

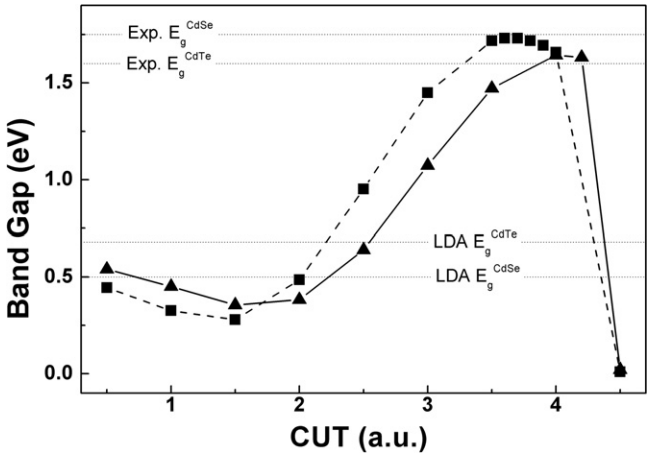

Fig. 1. Variational determination of the CUT parameter for the anions. Spin–orbit coupling was not included. Also shown are the horizontal lines representing experimental and LDA bandgaps.

3. Results

Fig. 2 shows the CdTe and CdSe band structures obtained with LDA and LDA-1/2. Without SO correction, the calculated wz-CdTe direct band gap is 1.78 eV, consistent with previous GW calculations [29]. SO effects reduce the band gap by 0.23–1.55 eV, in good agreement with the experimental value of 1.60 eV for wz–CdTe [30]. Unlike zb–CdTe, where the values we obtained for Δ_{SO} employing either LDA and LDA-1/2 PPs are quite close (0.87 and 0.85 eV, respectively, in good agreement with experimental values 0.90–0.95 eV [25,31,32]), for wz–CdTe we found a larger difference for the equilibrium splitting parameter Δ_{SO}, 0.85 and 0.76 eV, obtained with LDA and LDA-1/2, respectively. We have been unable to find experimental values for wz–CdTe to compare with. Our calculated direct band gap of wz–CdSe without SO coupling is 1.77 eV,

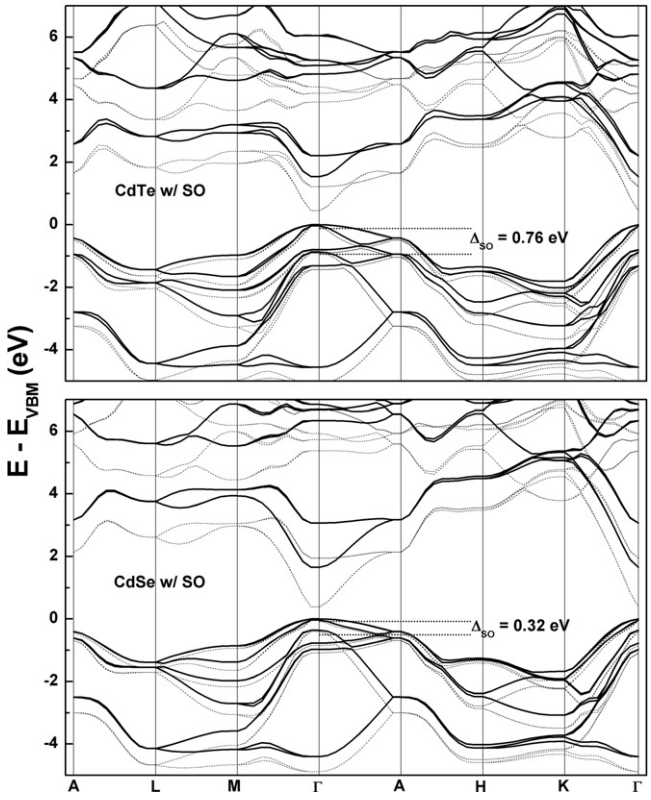

Fig. 2. LDA-1/2 (solid) and LDA (dotted) band structures for bulk wurtzite CdTe (top) and CdSe (bottom), both considering SO coupling. Self-energy correction changes very little the LDA SO energies but have a considerable impact on the LDA band gaps. Reference energy taken at the top of the valence bands.

Table 2
Bulk wurtzite CdSe and CdTe band gap energies without [E_g] and with [E_g(SO)] spin–orbit coupling. Also shown are the band splitting parameters Δ_{SO}. For comparison, band gap energies for strained structures including spin–orbit [$E_g^{blk\,str}$(SO)] were obtained from bulk LDA-1/2 calculations of CdSe (CdTe) strained to the CdTe (CdSe) lattice parameters c and $a_\parallel$, and $a_\perp$ relaxed to its equilibrium value. Without strain, $a_\parallel = a_\perp$. Experimental values are shown for comparison [25].

	Bulk band gaps (eV)					
	CdTe			CdSe		
	LDA	LDA-1/2	Exp.	LDA	LDA-1/2	Exp.
E_g	0.68	1.78		0.50	1.77	
E_g(SO)	0.45	1.55	1.60	0.38	1.66	1.75
$E_g^{blk\,str}$(SO)		1.62			1.28	
Δ_{SO}	0.85	0.76	0.95[a]	0.36	0.32	0.39–0.41

[a] Measured at 300 K [25].

in good agreement with the experimental band gap of 1.75 eV. The inclusion of SO coupling reduces the CdSe band gap to 1.66 eV, a decrease of only 0.11 eV, about half the decrease obtained for CdTe. SO correction to the CdSe band structure was also included by other authors employing semi-empirical methods [33–35], DFT [36], and GW [29]. Our LDA and LDA-1/2 values for Δ_{SO} for wz–CdSe are quite similar, 0.36 eV and 0.32 eV respectively, while the experimental results vary in the range 0.39–0.41 eV [25,37,38].

Table 2 summarises the effects of LDA-1/2 and SO energy corrections on the bulk band gaps of bulk wz–CdTe and wz–CdSe. Notice that Δ_{SO} is about twice the LDA band gap energy E_g(SO) for CdTe, and close to the value of E_g(SO) for CdSe. The table also shows the value of the band gaps under strain, $E_g^{blk\,str}$, where the $a_\parallel$ and c LVs of the CdTe (CdSe) bulk were fit to the CdSe (CdTe) bulk values, while the normal vector $a_\perp$ was relaxed. Under strain the band structures

Table 3
Strained CdSe and CdTe bulk and heterostructure LDA-1/2 band gaps. *blk str* values refer to bulk CdTe (CdSe) strained to the CdSe (CdTe) c and $a_\parallel$ lattice vectors, with $a_\perp$ lattice vector relaxed to its equilibrium value. Without strain, $a_\parallel = a_\perp$. *het* is similar to *blk str* except that the band gaps were obtained from heterostructure calculations.

Effect of strain on band gaps (eV)		
$E_g^{blk\,str}$	CdSe:	1.77
	CdTe:	1.87
E_g^{het}	CdSe:	1.64
	CdTe:	1.82

undergo considerable changes. For strained CdSe the LDA band gap changes to indirect within LDA-1/2. On the other hand, with LDA-1/2 strained CdSe displays a direct band gap as in the unstrained case, with a strained band gap value of 1.28 eV.

We emphasise that the biaxial strain employed was such that the CdTe cell had the c and $a_\parallel$ lattice vectors of the other (≈ 6 % lattice mismatch), while the $a_\perp$ lattice vector was relaxed, releasing some of the strain energy. Of course $a_\parallel = a_\perp$ without strain. Under compressive strain, CdTe increases its energy bandgap as expected. The impact of strain in the band gap (without SO) of the bulk CdTe is summarised in Table 3.

In the heterostructure configuration, CdSe is considered as the substrate and CdTe is lattice matched to it as a thin film. The atomic positions are relaxed to get a more precise charge mixing at the interface. To guarantee that the interfaces are far enough to avoid interactions and charge confinement, 64 atomic planes of each material were included in the model. This number of planes was the minimum necessary to obtain well converged band offsets from the density of states projected on the atomic planes (PDOS), which is useful to investigate the band edges along the transition region between the two materials. Table 3 shows that for these many planes quantum confinement is minimised resulting in heterostructure band gaps (obtained as far as possible from the interfaces) in good agreement with their corresponding bulk values. The difference between bulk and heterostructure band gaps is not larger than 0.13 eV, indicating good convergence.

The band offsets were calculated with the method of PDOS onto atomic planes, similar to Louie *et al.* [39] and Bass *et al.* [40]. From the PDOS taken from each atomic plane we can obtain the profiles for VBM and CBM across the heterostructure from CdTe to CdSe. For each plane (z value), we identify one band edge by imposing that the number of states from the clean midgap region to the edge in question is greater than a limit value. In our cases, a threshold of 3E-4 states/plane was determined when the eigenvalues of the band edges in a plane far from the interface recover approximately the bulk band gap.

Fig. 3 shows the variation of the LDA-1/2 band gaps and band offsets along the heterostructure, in comparison to the LDA, from CdTe (left) to CdSe. As expected the CdSe valence band edges (VBE) are lower in energy than in CdTe due to Se higher electronegativity number if compared to Te. The conduction band edges (CBE) alignment forms the staggered band offset of this junction. SO effects investigated in the bulk calculations are not included here due to high computational cost. Due to the staggered band alignment, the heterostructure CBE (VBE) is composed of CdSe (CdTe) wave functions. Notice that the VBE transition profile from CdSe to CdTe is somewhat faster than the CBE transition in the opposite direction. Moreover, the CBE transition occurs entirely in the CdTe side of the interface, while the VBE transition occurs entirely in the CdSe side, revealing the greater localisation of the valence (conduction) band edges along the interface at the CdTe (CdSe) side. Fig. 3 also shows that the electronic transition region spans 24 atomic planes, or ≈61.4 Å, and is nearly centred at the physical interface. Because the transition regions for the CBE and VBE span several atomic plane, the band gap along the transition region varies non-monotonically,

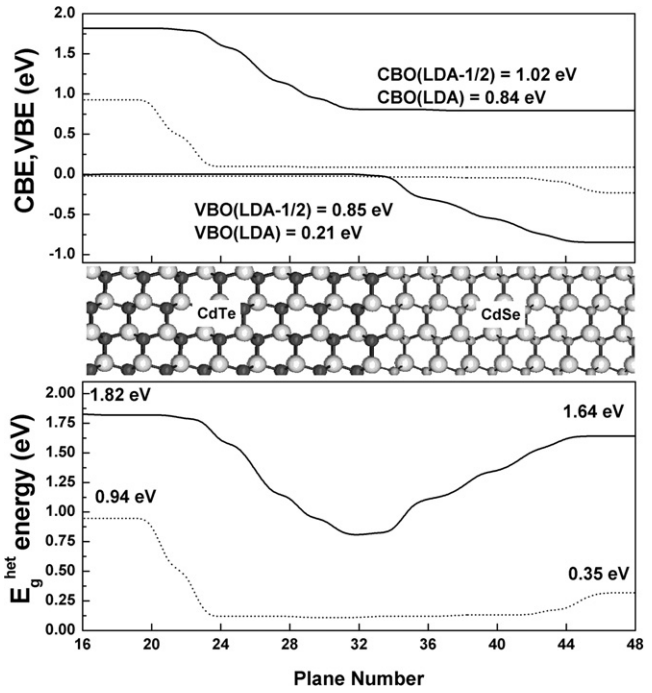

Fig. 3. Top: LDA and LDA-1/2 conduction and valence band edges along the heterojunction, from CdTe (left) to CdSe. Valence and conduction band offsets (VBO and CBO) are indicated. Mean inter-planar distances ≈1.92 Å; middle: heterostructure model (light grey: Cd; grey: Se; dark grey: Te); bottom: LDA and LDA-1/2 band gaps (E_g^{het}) along the heterojunction, from CdTe (left) CdSe. Solid and dotted lines in top and bottom panels correspond to LDA-1/2 and LDA calculations, respectively. SO effects not included.

ranging from ≈ 0.76 (0.82) eV near the interface to 1.64 eV in the CdSe side and 1.82 eV in the CdTe side. Such spectrum seems to be particular to the CdSe/CdTe interface, since similar calculations of the Si/SiO_2 [15] and GaAs/AlAs [16] interfaces yielded monotonic band gap variation in the transition region. The ≈ 0.8–1.8 eV band gap variation of the CdSe/CdTe interface band gap over the ≈61.4 Å transition region may lead to a reinterpretation of light absorption data by this system since the heterostructure may be more efficient at absorbing low frequency radiation than anticipated. Moreover, a band gap smaller around the interface than in the bulk regions of CdSe and CdTe implies in larger dielectric constants in that region. As a consequence, the associated refractive index around the interface will be larger. As this structure could act as an optical inhibitor to higher energy photons around the interface, a coaxial CdSe/CdTe nanowire could act as an optical waveguide for a particular frequency range as well.

Table 4 summarises the band offsets of the CdSe/CdTe heterostructure considered, comparing LDA and LDA-1/2 results. LDA-1/2-derived VBO is more than a factor of two larger than corresponding LDA value, while for the CBO the difference is ranges from 1.2 times larger than obtained with LDA. Here the bulk SO calculated energies add to the VBO results just about 0.1 eV both for LDA and LDA-1/2, thanks to the strain. Our CBO bigger than the VBO indicates a higher barrier for electrons than for holes. If the band gap reduction for CdTe and CdSe due to spin–orbit are ∼0.25 and ∼0.1, respectively, then the new VBO would be their difference, *i.e.* 0.15 eV. This is an estimate of the maximum difference in the VBO if the bulk spin–orbit energies were considered in the strained interface.

Table 4
LDA-1/2 and LDA band offsets for the CdSe/CdTe heterostructure configuration.

	Band offsets (eV)	
	LDA-1/2	LDA
CBO	1.02	0.84
VBO	0.85	0.21

4. Conclusions

We have calculated the wurtzite CdSe and CdTe bulk electronic band gaps and their interface band offsets using spin-unpolarised self-energy DFT/LDA-1/2 technique. The bulk band gap energies including SO effects are in good agreement with experiments. Assuming strained CdTe over relaxed CdSe, we found that the conduction and valence band offsets span an ≈61 Å long region surrounding the interface, with the conduction band transition occurring mostly in the CdTe side of the interface and the valence band transition occurring mostly in the CdSe side of the interface. As result, the band gap transition is not monotonic, reaching a minimum near the interface before converging to its bulk values at each side of the interface. The band gap ranges between 0.8 and 1.8 eV along the transition region. This behaviour may have important consequences for the mechanism of light absorption at the interface between these two materials in photovoltaic applications, as the small band gap should improve the performance of the device for longer wavelengths. We found that spin–orbit coupling energies are significant for the bulk band gaps of the two materials, but do not affect considerably the band offsets. The LDA-1/2 technique reproduces well the expected band alignment type for this interface, thus opening a new possibility for applications in more complex systems as photovoltaic interfaces in nanostructures.

Acknowledgements

MRJ thanks M. Marques, L. Teles and J. Furthmüller for appreciated discussions and Brazilian agency CAPES for financial support. LGF acknowledges FAPESP and CNPq for financial support. This work was done with the computational resources of the Instituto Tecnológico de Aeronáutica (FAPESP grant 2006/05858-0) and of the LCCA-Laboratory of Advanced Scientific Computation of the University of São Paulo. MRJ and LRCF thank D. Thober and Semp-Toshiba for financial support.

References

[1] A.J. Nozik, Inorg. Chem. 44 (2005) 6893.
[2] R.D. Schaller, V.I. Klimov, Phys. Rev. Lett. 92 (2004) 186601.
[3] N.S. Lewis, Science 315 (2007) 798.
[4] S. Neretina, R.A. Hughes, J.F. Britten, N.V. Sochinskii, J.S. Preston, P. Mascher, Nanotechnology 18 (2007) 275301.
[5] X. Peng, M.C. Schlamp, A.V. Kadavanich, A.P. Alivisatos, J. Am. Chem. Soc. 119 (1997) 7019.
[6] P. Hohenberg, W. Kohn, Phys. Rev. 136 (1964) B864.
[7] W. Kohn, L.J. Sham, Phys. Rev. 140 (1965) A1133.
[8] C. Delerue, M. Lannoo, Nanostructures Theory and Modelling, Springer-Verlag, 2004.
[9] C. Fiolhais, F. Nogueira, M. Marques (Eds.), A Primer in Density Functional Theory, 1st ed., Springer, New York, 2002.
[10] S. Yang, D. Prendergast, J.B. Neaton, Nano Lett. 10 (2010) 3156.
[11] S. Wang, L.-W. Wang, J. Phys. Chem. Lett. 2 (2011) 1.
[12] S. Gundel, A. Fleszar. W. Faschinger, W. Hanke., Phys. Rev. B 59 (1999) 15261.
[13] L.G. Ferreira, M. Marques, L.K. Teles, Phys. Rev. B 78 (2008) 125116.
[14] L.G. Ferreira, M. Marques, L.K. Teles, AIP Adv. 1 (2011) 032119.
[15] M. Ribeiro Jr., L.R.C. Fonseca, L.G. Ferreira, Phys. Rev. B 79 (2009) 241312(R).
[16] M. Ribeiro Jr., L.R.C. Fonseca, L.G. Ferreira, Europhys. Lett. 94 (2011) 27001.
[17] T. Sadowski, R. Ramprasad, J. Phys. Chem. C 114 (2010) 1773.
[18] D.K. Ward, X.W. Zhou, B.M. Wong, F.P. Doty, J.A. Zimmerman, J. Chem. Phys. 134 (2011) 244703.
[19] J. Matthews, A. Blakeslee, J. Cryst. Growth 27 (1974) 118.
[20] X. Zhang, S. Wang, D. Ding, X. Liu, J.-H. Tan, J. Furdyna, Y.-H. Zhang, D. Smith, J. Electron. Mater. 38 (2009) 1558.
[21] J.P. Perdew, A. Zunger, Phys. Rev. B 23 (1981) 5048.
[22] G. Kresse, D. Joubert, Phys. Rev. B 59 (1999) 1758.
[23] G. Kresse, J. Furthmüller, VASP the Guide. http://cms.mpi.univie.ac.at/vasp/guide/vasp.html.

[24] H.J. Monkhorst, J.D. Pack, Phys. Rev. B 13 (1976) 5188.
[25] O. Madelung (Ed.), Data Handbook, Springer, 2004.
[26] R.R. Pelá, C. Caetano, M. Marques, L.G. Ferreira, J. Furthmüller, L.K. Teles, Appl. Phys. Lett. 98 (2011) 151907.
[27] J.C. Slater, Adv. Quantum Chem. 6 (1972) 1.
[28] J.C. Slater, K.H. Johnson, Phys. Rev. B 5 (1972) 844.
[29] O. Zakharov, A. Rubio, X. Blase, M.L. Cohen, S.G. Louie, Phys. Rev. B 50 (1994) 10780.
[30] K. H. Hellwege, O. Madelung (Eds.), Numerical Data and Functional Relationships in Science and Technology, Landolt-Börnstein, New Series, Group III, vol. 17, part A and vol. 22, part A, Springer, 1982.
[31] H.C. Poon, Z.C. Feng, Y.P. Feng, M.F. Li, J. Phys.: Condens. Matter 7 (1995) 2783.
[32] S. Bloom, T.K. Bergstresser, Solid State Comm. 6 (1968) 465.
[33] A. Kobayashi, O.F. Sankey, S.M. Volz, J.D. Dow, Phys. Rev. B 28 (1983) 935.
[34] D.J. Stukel, R.N. Euwema, T.C. Collins, F. Herman, R.L. Kortum, Phys. Rev. 179 (1969) 740.
[35] T.K. Bergstresser, M.L. Cohen, Phys. Rev. 164 (1967) 1069.
[36] X. Chen, X. Hua, J. Hu, J.-M. Langlois, W.A. Goddard, Phys. Rev. B 53 (1996) 1377.
[37] Y.D. Kim, M.V. Klein, S.F. Ren, Y.C. Chang, H. Luo, N. Samarth, J.K. Furdyna, Phys. Rev. B 49 (1994) 7262.
[38] O. Portillo-Moreno et al. Opt. Mater. 18 (2002) 383.
[39] S.G. Louie, M.L. Cohen, Phys. Rev. Lett. 35 (1975) 866.
[40] J.M. Bass, M. Oloumi, C.C. Matthai, J. Phys.: Condens. Matter 1 (1989) 10625.